J. Chem. Sci. Vol. 129, No. 9, September 2017, pp. 1373–1380.
DOI 10.1007/s12039-017-1344-9

REGULAR ARTICLE

Liquid-phase oxidation of naphthalene with H_2O_2 in the presence of ordered mesoporous V-*m*-Al_2O_3 catalysts

ZHIWEI ZHOU[a], YANG YU[a], JUAN QIN[b], JIAQI ZHANG[a], FULIN CHENG[a] and WENLIANG WU[a,*]

[a]College of Chemical Engineering, Nanjing Tech University, Nanjing 210009, People's Republic of China
[b]Technology and Finance Service Center of Jiangsu Province, Productivity Center of Jiangsu Province, Nanjing 210042, People's Republic of China
E-mail: wwl@njtech.edu.cn

MS received 31 December 2016; revised 21 March 2017; accepted 14 June 2017; published online 3 August 2017

Abstract. The ordered mesoporous V-*m*-Al_2O_3 catalysts were successfully synthesized *via* a facile one-pot evaporation-induced self-assembly (EISA) strategy and applied in the liquid-phase oxidation of naphthalene with hydrogen peroxide in the presence of ascorbic acid as a reductant. The physicochemical properties of the catalysts were investigated using various techniques, like XRD, N_2 sorption, UV-Vis spectra, Raman spectroscopy, XPS, XRF and TEM. Small-angle XRD, N_2 sorption and TEM results show that mesoporous V-*m*-Al_2O_3 catalysts possess a highly ordered mesostructure with large surface areas and narrow pore-size distributions. High-angle XRD, UV-Vis spectra and Raman spectroscopy results indicate that VO*x* species were homogeneously incorporated in the matrix of mesoporous Al_2O_3.The catalytic performance in the liquid oxidation of naphthalene with H_2O_2 over 8V-*m*-Al_2O_3 catalyst (naphthalene conversion 45.4% and phthalic anhydride selectivity 61.0%) was higher than other catalysts. The vanadium species incorporated in the 8V-*m*-Al_2O_3 sample were stable, and its catalytic stability was kept well even after repeated use for 5 times, which indicates a green and economical pathway for naphthalene degradation.

Keywords. Ordered mesoporous Al_2O_3; vanadium; EISA; naphthalene oxidation; phthalic anhydride.

1. Introduction

Naphthalene, a member of polycyclic aromatic hydrocarbons (PAHs), is an environmental pollutant.[1,2] In the past decades, many techniques, such as biodegradation, photocatalysis and aerobic catalytic oxidation, have been exploited for its elimination.[3–5] Owing to lower efficiency and higher time consumption by the former two methods, the aerobic catalytic oxidation may be the most promising approach. However, catalytic oxidation in gas-phase is usually adopted and carbon dioxide is the final product. This process not only aggravates the greenhouse effect but also causes wastage of resource.[6,7] Therefore, it is essential to explore new approaches to transform naphthalene to some fine chemicals with high values.

Since the discovery of mesoporous silica-based materials in the 1990s, it has attracted extensive attention.[8,9] However, its poor hydrothermal stability and lack of catalytic active sites hinder its industrial application.[10] Liquid-phase oxidation of naphthalene for the preparation of fine chemicals has been exploited over mesoporous silica-based materials, such as Fe-SBA-15, V-MCM-41, Fe-SiO_2, and Mn(TF_5PP)-MCM-41.[11–14] But their catalytic activities were low and time-consuming catalyst preparation procedure was required. Compared to the mesoporous silica-based materials, the non-siliceous mesoporous materials such as mesoporous metal oxides and heteroatom zeolites have recently been proposed as potential catalysts in many catalytic industries.[15,16] As a typical metal oxide, ordered mesoporous alumina has already been applied in many industrial catalytic reactions, such as petroleum refinement, oxidation reaction and other fine chemical industry.[17–19] Mesoporous alumina-supported metal oxides prepared by the one-pot method can achieve

*For correspondence

Electronic supplementary material: The online version of this article (doi:10.1007/s12039-017-1344-9) contains supplementary material, which is available to authorized users.

high-quality mesostructures, which can retain homogeneous distribution of active sites.[20,21] Vanadium containing catalysts have proved to be the most promising catalytic systems for oxidation reactions.[22] Therefore, vanadium species incorporated into the matrix of mesoporous alumina prepared by one-pot method would show high catalytic performance in the liquid-phase oxidation of naphthalene. Also, it is rarely reported so far.

In this work, the ordered mesoporous V-*m*-Al_2O_3 catalysts were prepared by the facile EISA method and their catalytic behavior in the liquid-phase catalytic oxidation of naphthalene with hydrogen peroxide was investigated in this paper. The textural structure and physical properties of different V-*m*-Al_2O_3 catalysts were studied using XRD, N_2 sorption, UV-Vis spectra, Raman spectroscopy and TEM technique. The reusability of catalyst was also investigated.

2. Experimental

2.1 *Synthesis of ordered mesoporous V-m-Al_2O_3 catalysts*

The ordered mesoporous V-*m*-Al_2O_3 catalysts were prepared by a modified EISA method according to the reference.[20] In a typical synthesis process, 1.0 g P123 and stoichiometric amounts of vanadyl acetylacetonate were dissolved in 20.0 mL anhydrous ethanol, followed by the addition of 2.04 g aluminum iso-propoxide under vigorous stirring. Then 1.6 mL nitric acid (67 wt.%) was dropped into the mixture and stirred for 6 h at room temperature. The sol was subsequently transferred to a petri dish and dried at 60°C for 48 h. The final samples were obtained after the gel was calcined at 600°C for 5 h in air and designated as *x*V-*m*-Al_2O_3 (x = 0, 2, 5, 8, 10 and 12), where x represents the molar ratio of vanadium species to aluminum species. For comparison, the 8V-Al_2O_3-c and 8V-Al_2O_3-i samples were prepared by co-precipitation and impregnation methods, respectively.

2.2 *Catalysts characterization*

The XRD patterns were obtained on a Rigaku Smartlab instrument with Ni-filtered Cu Kα radiation (λ = 0.154 nm) and operated at 40 kV and 40 mA. The scanning step was 0.02° in the range from 0.5° to 5° (small-angle range) and from 10° to 80° (wide-angle range). N_2 sorption isotherms were measured at −196°C using a BELSORP-MINI volumetric adsorption analyzer. The samples were degassed at 200°C for 2 h under vacuum before measurement. The surface area was calculated according to BET method, and the pore size distribution was determined based on the BJH adsorption model from the adsorption isotherm branch. TEM image was recorded on the JEOL JEM-2010 EX transmission electron microscope under 200 kV. Before TEM measurement, the samples were dispersed in ethanol, assisted by an ultrasonic technique. UV-Vis diffuse reflectance spectra of the samples were measured in a Lambda 950 spectra analysis instrument in the range 200–800 nm using $BaSO_4$ as the reference. The absorbance was defined as log (1/T), where T is the transmittance. The thickness of solid film samples is 0.5 mm. The Raman measurements were performed on a LabRAM HR-800 with laser excitations at 514.5 nm. The surface chemical composition was analyzed by XPS conducted on the Thermo Scientific Escalab 250Xi spectrometer with Al K α X-ray source (1486 eV). The weight percent of different component in the catalysts was performed using the Switzerland ARL9800 XRF techniques.

2.3 *Catalytic tests*

The catalytic performance of the synthesized catalysts was carried out in a three-neck flat-bottom flask equipped with a reflux condenser at atmospheric pressure. In a typical process, 1 g of naphthalene, 0.1 g of catalyst and 0.05 g of ascorbic acid were simultaneously added into 20 g of acetonitrile as solvent and the mixture was kept stirring for 10 min. Then, 5 g of H_2O_2 (30 wt.%) was added into the reaction system through a syringe, and the mixture was kept stirring for 6 h at 60°C. At the completion of the reaction, the flask was cooled down to room temperature. The reaction mixture was analyzed on an SP-6890 gas chromatograph equipped with OV-1701 column and a flame ionization detector (FID). For the catalyst recyclability tests, the catalyst was separated by centrifugation after 6 h reaction time and washed with acetonitrile and ethanol, then dried at 110°C for 4 h before reusing.

3. Results and Discussion

3.1 *Catalyst characterization*

Low-angle XRD (LXRD) and wide-angle XRD (WXRD) patterns of different V-*m*-Al_2O_3 samples are shown in Figure 1. As can be seen from Figure 1 (A), a strong diffraction peak centered at around 1.0° and one weak peak centered at around 1.8° are observed for the *m*-Al_2O_3 sample, which can be attributed to *p6mm* hexagonal symmetry, suggesting it is long-range ordered and mesoporous.[15] The peak centered at 1.8° disappeared after the incorporation of the vanadium species, and the intensity of the peak centered at 1.0° decreased with the vanadium species loading increasing, indicating that its long-range ordered mesostructure is slightly collapsed. Figure 1 (B) displays the wide-angle XRD patterns of different V-*m*-Al_2O_3 samples. It can be seen that the amorphous aluminum oxide can be formed when the molar ratio of vanadium species to aluminum species is less than 8%. With the further increase in vanadium species, three diffraction peaks centered at

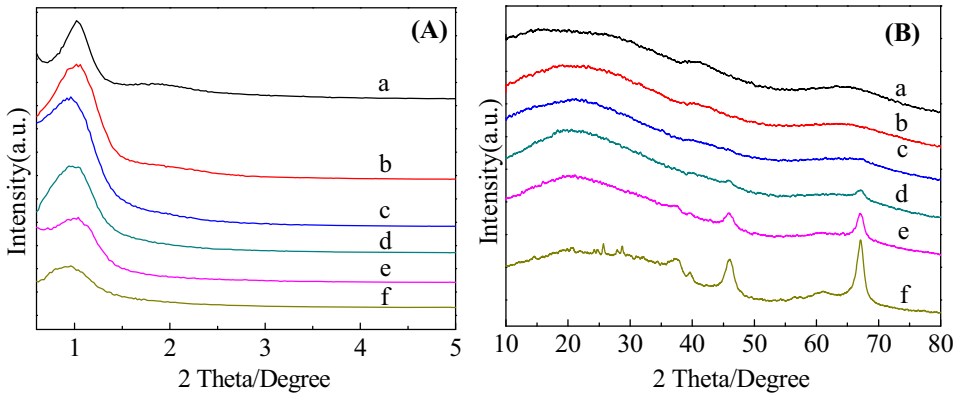

Figure 1. (A) Low-angle and (B) wide-angle XRD patterns of (a) *m*-Al_2O_3, (b) 2V-*m*-Al_2O_3, (c) 5V-*m*-Al_2O_3, (d) 8V-*m*-Al_2O_3, (e) 10V-*m*-Al_2O_3, (f) 12V-*m*-Al_2O_3.

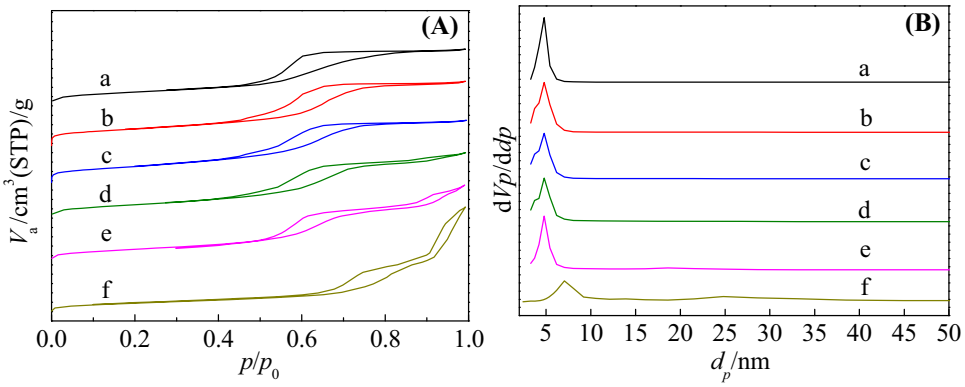

Figure 2. (A) N_2 sorption isotherms and (B) pore size distribution curves of (a) *m*-Al_2O_3, (b) 2V-*m*-Al_2O_3, (c) 5V-*m*-Al_2O_3, (d) 8V-*m*-Al_2O_3, (e) 10V-*m*-Al_2O_3, (f) 12V-*m*-Al_2O_3.

$2\theta = 37.6, 45.8$ and $67.0°$ are observed, suggesting that the crystal γ-Al_2O_3 (JCPDS Card No. 10-0425) were gained owing to the increasing presence of bulky acetylacetone ligand, probably.[17,23] However, no diffraction peak of VO*x* crystalline phase is detected, indicating that vanadium species is highly dispersed in the framework of mesoporous Al_2O_3. The 8V-Al_2O_3-c sample prepared by co-precipitation method showed distinct crystal γ-Al_2O_3 phase. Three new peaks centered at $2\theta =$ 25.7, 27.7 and 28.6° corresponding to diffraction peaks of $AlVO_4$ (JCPDS Card No. 39-0276) are observed in 8V-Al_2O_3-i sample (Figure S1, Supplementary information). The results further indicate that the EISA method is superior to another method in controlling Al_2O_3 crystal growth and the dispersion of vanadium species.

The N_2 sorption isotherms as well as the corresponding pore size distributions for different V-*m*-Al_2O_3 samples are shown in Figure 2 and the detailed textural properties are listed in Table 1. As shown in Figure 2 (A), the isotherms for V-*m*-Al_2O_3 samples, whose molar ratio of vanadium species to aluminum species was less than 8%, are type IV isotherms according to IUPAC classification and exhibit a H2 hysteresis loop, which is typical for mesoporous materials.[24] The hysteresis loop would be distorted and gradually shifted to higher pressure with the increase in vanadium species loading because of the formation of γ-Al_2O_3 phase resulting in its partial destruction of ordered Mesopores, probably, which agreed well with XRD patterns.[16] As seen in Table 1, the 8V-*m*-Al_2O_3 sample, with BET surface area of 176 m^2/g and pore volume of 0.28 cm^3/g, is optimal over other V-*m*-Al_2O_3 samples, indicating its potential for high catalytic performance. Compared to 8V-*m*-Al_2O_3 and 8V-Al_2O_3-i samples, the 8V-Al_2O_3-c sample showed a hysteresis loop at higher pressure and a wider pore diameter distribution owing to the stacking mesoporous structure, which would result in its lower surface area and pore volume (Figures S2, S3 and Table S1). In addition, the surface area, pore diameter and volume for the 8V-Al_2O_3-i sample prepared by impregnation method are much lower than that of 8V-*m*-Al_2O_3 sample probably due to the partial blocking of mesopores by vanadium species.

Table 1. Physical properties of mesoporous V-*m*-Al_2O_3 catalysts.

Samples	Pore size (nm)[a]	S_{BET} ($m^2 \cdot g^{-1}$)[b]	Pore volume ($cm^3 \cdot g^{-1}$)[c]
m-Al_2O_3	4.8	152	0.24
2V-*m*-Al_2O_3	4.8	159	0.26
5V-*m*-Al_2O_3	4.8	166	0.26
8V-*m*-Al_2O_3	4.9	176	0.28
10V-*m*-Al_2O_3	5.1	149	0.33
12V-*m*-Al_2O_3	7.0	119	0.48

[a]BJH method; [b]BET specific areas; [c]$P/P_0 = 0.99$.

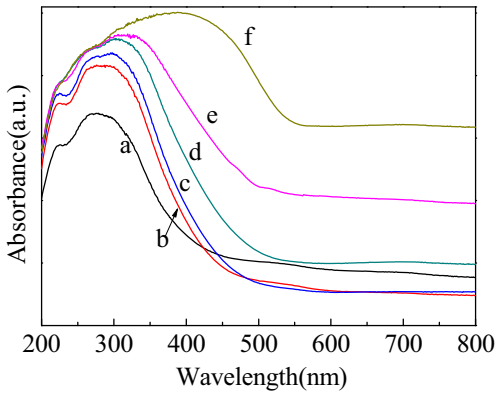

Figure 3. Diffuse reflection UV-Vis spectra of (a) *m*-Al_2O_3, (b) 2V-*m*-Al_2O_3, (c) 5V-*m*-Al_2O_3, (d) 8V-*m*-Al_2O_3, (e) 10V-*m*-Al_2O_3, (f) 12V-*m*-Al_2O_3.

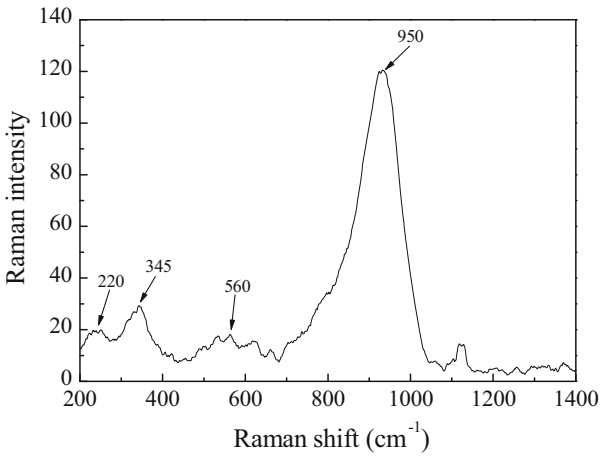

Figure 4. Raman spectra of 8V-*m*-Al_2O_3 samplewith laser excitations at 514.5 nm.

Figure 3 presents the UV-Vis spectra of different V-*m*-Al_2O_3 samples. Two bands, one centered at 220 nm and another centered at 270 nm, were observed for pure *m*-Al_2O_3 sample, which is in good agreement with literature.[25] However, compared to the pure *m*-Al_2O_3 sample, the intensity of absorption band in the region 280–290 nm increases with the incorporation of vanadium species. This increase can be attributed to the formation of isolated tetrahedral vanadium species.[26] At the same time, with the amount of the vanadium species increasing, a red-shifted absorption band in the region from 300 to 330 nm was observed owing to the polymeric tetrahedral vanadium species. For the sample 10V-*m*-Al_2O_3, a weak absorption band in the region 400–450 nm was observed, which can be attributed to octahedral V^{5+} species.[27] Similarly, the band increases distinctly for 12V-*m*-Al_2O_3 sample, which can also be attributed to microcrystalline V_2O_5 species. Compared to 8V-*m*-Al_2O_3 sample, the absorption band in the region 400–450 nm corresponding to octahedral V^{5+} species for 8V-Al_2O_3-i and 8V-Al_2O_3-c samples can also be observed (Figure S4), which indicate further formation of extra-framework vanadium species. Furthermore, the band increases distinctly for 8V-Al_2O_3-i sample, which can be assigned to the microcrystalline V_2O_5 species not detected by XRD patterns.

Raman spectroscopy is a useful technique providing information about the various types of vanadium species that are not detected by XRD patterns. The Raman lines below 900 cm^{-1} would be assigned to the vibration of polymeric V-O-V species, and the Raman lines in the region from 900 to 1000 cm^{-1} can be identified with the V=O stretch vibration of polymeric vanadium species.[28] Figure 4 shows the Raman spectra of 8V-*m*-Al_2O_3 sample. It can be seen in Figure 4 that a major Raman line at around 950 cm^{-1} is observed accompanied by weak lines at ~560, ~345 and ~220 cm^{-1}. This indicates that the polymeric tetrahedral vanadate, undetectable by the XRD patterns, is the major component of vanadium species after its incorporation into the structure of *m*-Al_2O_3.[29,30]

Figure 5 shows the TEM images for 8V-*m*-Al_2O_3 catalyst. The typical long-range ordered mesostructure was obviously observed, which is in good agreement with the intense XRD peak shown in small-angle XRD patterns. The high dispersion of VO*x* species in the matrix of *m*-Al_2O_3 is shown in the high-resolution TEM image.

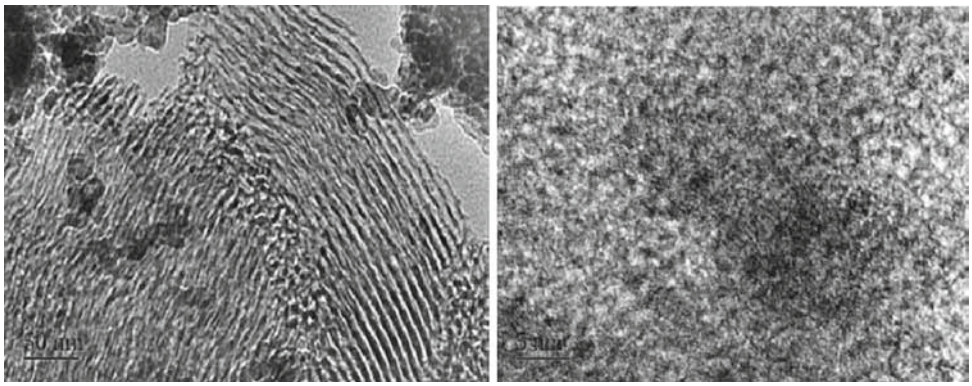

Figure 5. TEM images of 8V-*m*-Al_2O_3 sample.

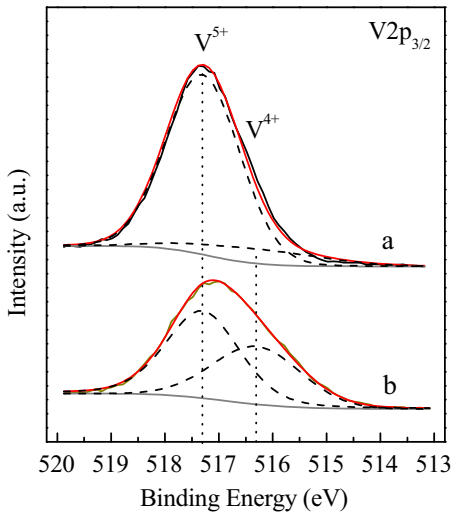

Figure 6. XPS spectra for (a) fresh and (b) reduced 8V-*m*-Al_2O_3 catalysts.

Figure 6 shows XPS spectra for 8V-*m*-Al_2O_3 catalysts in its two states, fresh sample (Figure 6a) and reduced by ascorbic acid (Figure 6b). A major peak centered at 517.3 eV corresponding to V^{5+} species and another small peak centered at 516.3 eV corresponding to V^{4+} species for fresh 8V-*m*-Al_2O_3 catalyst are observed, suggesting that the V^{5+} species was predominantly formed.[31,32] However, the peak area of V^{4+} species distinctly increased for the reduced catalyst by ascorbic acid. This indicated that the high valence vanadium species are reduced to low valence by ascorbic acid, which are the active sites for the oxidation of naphthalene.

3.2 *Catalytic performance*

Table 2 summarizes the catalyst performance of different V-*m*-Al_2O_3 catalysts in the liquid-phase oxidation of naphthalene with hydrogen peroxide in the presence of ascorbic acid as the reductant and acetonitrile as the solvent. The major products are phthalic anhydride and 1,4-napthaquinone. No naphthalene conversion was observed over pure *m*-Al_2O_3 catalyst. Compared to the pure *m*-Al_2O_3 catalyst, the conversion of naphthalene could be detected, and it increased with the loading of vanadium species, increasing from the molar ratio 2 to 8, where the naphthalene conversion is as high as 45.4% and the selectivity of phthalic anhydride is maximum 61.1%; probably, owing to its long-range ordered mesostructure, high surface area, and appropriate pore volume and size. With further increase in vanadium species loading, both the naphthalene conversion and the selectivity of phthalic anhydride decreased, suggesting that the isolated tetrahedral vanadium species are the main active sites.[12] In addition, the catalytic performance in the absence of ascorbic acid was also investigated, and the naphthalene conversion was 0.3%, which indicated that the ascorbic acid is essential to reduce the vanadium species with high valent to lower valent for the oxidation of naphthalene by hydrogen peroxide.[33] At the same time, naphthalene conversion for 8V-*m*-Al_2O_3 catalyst is much higher than other two samples, owing to its higher surface area and appropriate pore size and volume. The results further indicated that the EISA process is a promising method to prepare complicated metal oxides with ordered mesopores.

To test the heterogeneity of V-*m*-Al_2O_3 catalysts, leaching experiments were carried out according to previous reports.[13,34] The catalyst was removed at 0.5 h under the optimal reaction condition by centrifugation. Then, the filtrate was applied for further reaction under the same reaction condition. The results of leaching experiment are shown in Figure 7. It can be seen that the conversion of naphthalene at 0.5 h (before catalyst removal) was 18.2%. With the increasing of reaction time, a slight enhancement in naphthalene conversion was observed, which maybe owing to the little leached vanadium species dispersed on the support surface

Table 2. Catalytic performance of different V-*m*-Al_2O_3 catalysts in the liquid-phase oxidation of naphthalene.

Entry	Catalysts	Naphthalene conversion (%)	Selectivity (%)		
			Phthalic anhydride	1,4-naphthoquinone	Others
1	*m*-Al_2O_3	–	–	–	–
2	2V-*m*-Al_2O_3	8.0	48.7	33.3	18.0
3	5V-*m*-Al_2O_3	19.4	51.9	30.2	17.9
4	8V-*m*-Al_2O_3	45.4	61.0	27.6	11.4
5	10V-*m*-Al_2O_3	41.1	57.6	28.3	14.1
6	12V-*m*-Al_2O_3	37.1	54.2	30.3	15.5
7	Non Catalyst, Non Reductant	–	–	–	–
8	8V-*m*-Al_2O_3, Non Reductant	0.3	11.5	8.9	79.6
9	8V-Al_2O_3-c	18.0	42.3	45.2	12.5
10	8V-Al_2O_3-i	21.2	35.4	49.5	15.1

Reaction conditions: w(catalyst)/w(naphthalene) = 0.1; w(acetonitrile)/w(naphthalene) = 20; w(ascorbic acid)/w(catalyst) = 0.5;w(H_2O_2)/w(naphthalene) = 1.5; reaction time: 6 h; reaction temperature: 60°C.

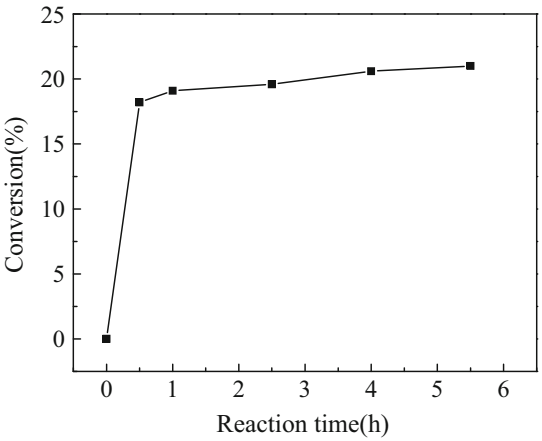

Figure 7. Leaching experiment of 8V−*m*−Al_2O_3 catalyst in the liquid-phase oxidation of naphthalene. Reaction conditions: w(catalyst)/w(naphthalene) = 0.1; w(acetonitrile)/w(naphthalene) = 20; w(ascorbic acid)/w(catalyst) = 0.5; w(H_2O_2)/w(naphthalene) = 1.5; reaction time: 6 h; reaction temperature: 60°C.

through the hydrogen bonding rather than incorporated species in the matrix of mesoporous Al_2O_3. The chemical composition of the fresh and filtered catalysts were analyzed by XRF techniques. Compared to a fresh catalyst, the vanadium content slightly decreased from 7.42 to 7.34 wt.%, which indicated that the vanadium species incorporated in the 8V-*m*-Al_2O_3 sample was stable and thereby resistant to leaching.

Table 3 shows the data on the reusability for 8V-*m*-Al_2O_3 catalyst in the liquid-phase oxidation of naphthalene. It was observed that the naphthalene conversion slightly decreased after the reuse for five times. Conversion of naphthalene 39.1% and selectivity of phthalic anhydride 57.6% was obtained, which suggested that the 8V-*m*-Al_2O_3 catalyst has good reusability implying its potential industrial application.

Therefore, based on the characterization and catalytic performance of V-*m*-Al_2O_3 catalyst above, a possible mechanism is proposed and shown in Scheme 1. Accordingly, it is suggested that ascorbic acid will help to reduce the high valent V^{5+} species in V-*m*-Al_2O_3 catalyst to V^{4+} species. This in turn will activate hydrogen

Table 3. Catalytic reusability of 8V-*m*-Al_2O_3 catalyst in the liquid-phase oxidation of naphthalene.

Entry	Naphthalene Conversion (%)	Selectivity (%)		
		Phthalic anhydride	1,4-naphthoquinone	Others
1	45.4	61.0	27.6	11.4
2	44.2	58.7	26.8	14.5
3	41.0	54.9	27.0	18.1
4	42.1	58.0	30.9	11.1
5	39.1	57.6	29.2	13.2

Reaction conditions: w(catalyst)/w(naphthalene) = 0.1; w(acetonitrile)/w(naphthalene) = 20; w(H_2O_2)/w(naphthalene) = 1.5; w(ascorbic acid)/w(catalyst) = 0.5; reaction time: 6 h; reaction temperature: 60°C.

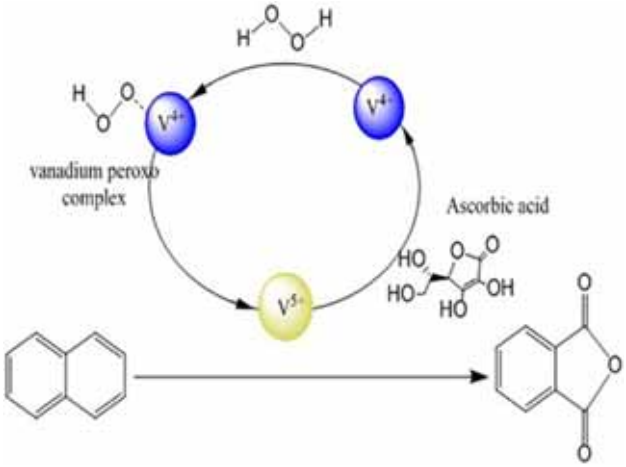

Scheme 1. Possible reaction mechanism for mesoporous V-*m*-Al_2O_3 catalyst in liquid-phase oxidation of naphthalene with hydrogen peroxide.

peroxide to produce active oxygen species to oxidize naphthalene to phthalic anhydride, while V^{4+} gets retransformed to V^{5+} species at the end of the catalytic cycle.

4. Conclusions

This paper reports the successful synthesis of V-*m*-Al_2O_3 by a modified one-pot EISA method. It was applied in the liquid-phase oxidation of naphthalene with hydrogen peroxide in the presence of ascorbic acid as reductant. Polymeric tetrahedral vanadate was formed and homogenously incorporated into the framework of *m*-Al_2O_3, which were the main active sites. The 8V-*m*-Al_2O_3 catalyst shows higher catalytic performance than other samples owing to its highest surface area, appropriate pore volume and size, whose naphthalene conversion and phthalic anhydride selectivity are 45.4% and 61.0%, respectively, and it has good reusability. At the same time, ascorbic acid is essential to reduce the vanadium species from high valent to lower valent for the oxidation of naphthalene by hydrogen peroxide.

Supplementary Information (SI)

The XRD, N_2 sorption, UV-*vis* spectra characterization for the 8V-Al_2O_3-c and 8V-Al_2O_3-i (Figures S1 to S4, Table S1) are given in the Supplementary Information, which is available at www.ias.ac.in/chemsci.

Acknowledgements

This work was supported by Jiangsu Planned Projects for Post-doctoral Research Funds (1302121C); Open Project of Beijing Key Laboratory for Enze Biomass and Fine Chemicals; Project Funded by the Priority Academic Program Development of Jiangsu Higher Education Institutions.

References

1. Clarke T J, Kondrat S A and Taylor S H 2015 Total oxidation of naphthalene using copper manganese oxide catalysts *Catal. Today* **258** 610
2. Aranda A, Puértolas B, Solsona B, Agouram S, Murillo R, Mastral A M, Taylor S H and Garcia T 2010 Total Oxidation of Naphthalene Using Mesoporous CeO_2 Catalysts Synthesized by Nanocasting from Two Dimensional SBA-15 and Three Dimensional KIT-6 and MCM-48 Silica Templates *Catal. Lett.* **134** 110
3. Jouanneau Y, Meyer C and Duraffourg N 2016 Dihydroxylation of four- and five-ring aromatic hydrocarbons by the naphthalene dioxygenase from Sphingomonas CHY-1 *Appl. Microbiol. Biot.* **100** 1253
4. Venkatathri N, Pillai V K, Rajini A, Raju M N and Reddy I A K 2013 Structural and catalytic properties of a novel vanadium containing solid core mesoporous silica shell catalysts for gas phase oxidation reaction *J. Chem. Sci.* **125** 63
5. Karuppiah J, Reddy E L, Sivachandiran L, Karvembu R and Subrahmanyam C 2012 Nonthermal plasma assisted photocatalytic oxidation of dilute benzene *J. Chem. Sci.* **124** 841
6. Bampenrat A, Meeyoo V, Kitiyanan B, Rangsunvigit P and Rirksomboon T 2008 Catalytic oxidation of naphthalene over CeO_2-ZrO_2 mixed oxide catalysts *Catal. Commun.* **9** 2349
7. Varela-Gandía F J, Ángel Berenguer-Murcia, Lozano-Castelló D, Cazorla-Amorós D, Sellick D R and Taylor S H 2013 Total oxidation of naphthalene using palladium nanoparticles supported on BETA, ZSM-5, SAPO-5 and alumina powders *Appl. Catal. B-Environ.* **129** 98
8. Kresge C T, Leonowicz M E, Roth W J, Vartuli J C and Beck J S 1992 Ordered mesoporous molecular sieves synthesized by a liquid-crystal template mechanism *Nature* **359** 710
9. Garg S, Soni K, Prasad V V D N, Kumar M, Bhaskar T, Gupta J K, Dhar G M and Gopinath C S 2014 Effect of method of preparation on hydrodesulphurization activity of Co- or Ni-promoted MoS_2/SBA − 15 catalysts *J. Chem. Sci.* **126** 437
10. Gómez S, Garces L J, Villegas J, Ghosh R, Giraldo O and Suib S L 2005 Synthesis and characterization of TM-MCM-48 (TM = Mn, V, Cr) and their catalytic activity in the oxidation of styrene *J. Catal.* **233** 60
11. Bangó A and Halász J 2009 Oxidation of condensed cyclic hydrocarbons with H_2O_2 in the presence of modified MCM-41 and SBA-15 mesoporous catalysts *React. Kinet. Mech. Cat.* **96** 413
12. Shylesh S and Singh A P 2004 Synthesis, characterization, and catalytic activity of vanadium-incorporated, -grafted, and -immobilized mesoporous MCM-41 in the oxidation of aromatics *J. Catal.* **228** 333
13. Andas J, Adam F, Rahman I A and Yun T Y 2014 Optimization and mechanistic study of the liquid-phase

oxidation of naphthalene over biomass-derived iron catalyst *Chem. Eng. J.* **252** 382
14. Yang F, Gao S, Xiong C, Wang H, Chen J and Kong Y 2015 Coordination of manganese porphyrins on amino-functionalized MCM-41 for heterogeneous catalysis of naphthalene hydroxylation *Chin. J. Catal.* **36** 1035
15. Morris S M, Fulvio P F and Jaroniec M2008 Ordered Mesoporous Alumina-Supported Metal Oxides *J. Am. Chem. Soc.* **130** 15210
16. Cai W, Yu J, Anand C, Vinu A and Jaroniec M 2011 Facile Synthesis of Ordered Mesoporous Alumina and Alumina-Supported Metal Oxides with Tailored Adsorption and Framework Properties *Chem. Mater.* **23** 1147
17. Liu Q, Gao J, Gu F, Lu X, Liu Y, Li H, Zhong Z, Liu B, Xu G and Su F 2015 One-pot synthesis of ordered mesoporous Ni-V-Al catalysts for CO methanation *J. Catal.* **326** 127
18. Gholampour N, Yusubov M and Verpoort F 2016 Investigation of the preparation and catalytic activity of supported Mo, W, and Re oxides as heterogeneous catalysts in olefin metathesis *Catal. Rev.* **58** 113
19. Hosseinzadeh R, Tajbakhsh M, Mohadjerani M and Mohammad A 2010 Copper-catalysed *N*-arylation of arylsulfonamides with aryl bromides and aryl iodides using KF/Al_2O *J. Chem. Sci.* **122** 143
20. Yuan Q, Yin A X, Luo C, Sun L D, Zhang Y W, Duan W T, Liu H C and Yan C H 2008 Facile synthesis for ordered mesoporous gamma-aluminas with high thermal stability *J. Am. Chem. Soc.* **130** 3465
21. Ham H, Kim J, Cho S J, Choi J H, Dong J M and Bae J W 2016 Enhanced Stability of Spatially Confined Copper Nanoparticles in an Ordered Mesoporous Alumina for Dimethyl Ether Synthesis from Syngas *ACS Catal.* **6** 5629
22. Li X H, Li W Y and Xie K C 2005 Supported Vanadia Catalysts for Dehydrogenation of Ethylbenzene with CO_2 *Catal. Lett.* **105** 223
23. Yuan H, Zhang C, Huo W, Ning C, Tang Y, Zhang Y, Cong D, Zhang W, Luo J, Li S and Wang Z 2014 Selective hydrogenation of maleic anhydride over Pd/Al_2O_3 catalysts prepared via colloid deposition *J. Chem. Sci.* **126** 141
24. Luo H Y, Zhang W, Zhou H W, Huang S Y, Lin P Z, Ding Y J and Lin L W 2011 A study of Rh-Sm-V/SiO_2 catalysts for the preparation of C_2-oxygenates from syngas *Appl. Catal. A-Gen.* **214** 161
25. Concepción P, Navarro M T, Blasco T, Nieto J M L, Panzacchi B and Rey F 2004 Vanadium oxide supported on mesoporous Al_2O_3: Preparation, characterization and reactivity *Catal. Today* **96** 179
26. Blasco T, Galli A, Nieto J M L and Trifiró F 1997 Oxidative Dehydrogenation of Ethane and *n*-Butane on VOx/Al_2O_3 Catalysts *J. Catal.* **169** 203
27. Eon J G, Olier R and Volta J C 1994 Oxidative Dehydrogenation of Propane on $\gamma - Al_2O_3$ Supported Vanadium Oxides *J. Catal.* **145** 318
28. Florea M, Marin R S, Pălăşanu F M, Neaţu F and Pârvulescu V I 2015 Mesostructured vanadia-alumina catalysts for the synthesis of vitamin K_3 *Catal. Today* **254** 29
29. Makgwane P R and Ray S S 2015 Development of a high-performance nanostructured V_2O_5/SnO_2 catalyst for efficient benzene hydroxylation *Appl. Catal. A-Gen.* **492** 10
30. Mannepalli L K, Dupati V, Vallabha S J and Manorama S V 2013 Synthesis of substituted guanidines using Zn-Al hydrotalcite catalyst *J. Chem. Sci.* **125** 1339
31. Bukallah S B, Bumajdad A, Khalil K M and Zaki M I 2010 Characterization of mesoporous VOx/MCM-41 composite materials obtained via post-synthesis impregnation *Appl. Surf. Sci.* **256** 6179
32. Carja G, Nakamura R, Aida T and Niiyama H 2003 Mg-V-Al mixed oxides with mesoporous properties using layered double hydroxides as precursors: catalytic behavior for the process of ethylbenzene dehydrogenation to styrene under a carbon dioxide flow *J. Catal.* **218** 104
33. Long Z, Zhou Y, Chen G, Zhao P and Wang J 2014 4,4'-Bipyridine-modified molybdovanadophosphoric acid: A reusable heterogeneous catalyst for direct hydroxylation of benzene with O_2 *Chem. Eng. J.* **239** 19
34. Reddy J S, Liu P and Sayari A 1996 Vanadium containing crystalline mesoporousmolecular sieves Leaching of vanadium in liquid phase reactions *Appl. Catal. A-Gen.* **148** 7